Nuclear Instruments and Methods in Physics Research B77 (1993) 110–116
North-Holland

NIM B
Beam Interactions with Materials & Atoms

Measurement of (p, p) elastic cross sections for C, O and Si in the energy range 1.0–3.5 MeV

R. Amirikas, D.N. Jamieson and S.P. Dooley
Microanalytical Research Centre, School of Physics, University of Melbourne, Parkville, Vic. 3052, Australia

Cross sections for the elastic scattering of protons from thin natural C, O and Si targets have been measured for proton bombarding energies between 1.0 and 3.5 MeV at lab angles of 170°, 150° and 110°. The results have been presented graphically and have been fitted with Breit–Wigner functions. The parameters of the fits are provided. These parameters may be used to simulate spectra from backscattering spectrometry (BS) analysis of sample composition. Some examples are shown for the measurement of SiC and YBaCuO superconductor stoichiometry.

1. Introduction

Proton elastic backscattering spectrometry (BS) is potentially a valuable analytical tool in micro-analysis of technological materials as well as biological and geological materials. Elastic scattering of protons by light nuclei is dominated by resonances which result from nuclear potential scattering in addition to Coulomb interaction. In general, highly non-Rutherford cross sections result above a bombarding energy of 1 MeV. Proton backscattering has different characteristics from α-particle backscattering. Protons have lower stopping cross sections and generally higher scattering cross sections for light elements than α-particles. Therefore, protons are more sensitive in detecting light elements. They also induce less radiation damage [1]. However, protons have poorer depth and mass resolution, but this is not necessarily a problem for analysis of light elements if the stoichiometry of the poorly resolved heavy elements is determined by α-particle BS or other methods.

The choice of protons as the projectile is often determined by the need to maximise the X-ray yield from the sample, as when trace elements to be measured by particle induced X-ray emission (PIXE). PIXE typically allows all elements above Na in the periodic table to be detected simultaneously and, usually, unambiguously. In this case, simultaneous detection of the backscattered protons can allow the lighter elements to be analysed, provided the scattering cross sections are known. For example, in a nuclear microprobe, proton BS can be used to image the distribution of the very light matrix elements in organic materials while PIXE is used to image the heavy trace elements. Thus PIXE and BS, implemented together, can provide a means for simultaneous microanalysis of both light and heavy elements. PIXE is typically performed with 2–3 MeV protons which is within the present range of measured proton cross sections.

However, to perform analysis with proton BS on light elements, it is necessary to have cross section data measured for the same detector geometry as that used in the analysis measurement. This is because the functional form of the cross sections is difficult to model analytically and the cross sections can have a strong angular dependence. Previous measurements of (p, p) cross sections, in the 50s and 60s, were usually to assign spin parities to nuclear energy levels and to obtain greater understanding of nuclear structure. The measurements were done with isotopically enriched targets and the results were presented graphically and in the centre of mass reference frame. Also the scattering angles were chosen such that the Legendre polynomial for a particular l value vanished and this was used for qualitative assignment of resonances. These cross sections are therefore not ideal for use in the analysis of natural samples. The previous work on cross section measurements is reviewed in refs. [2,3] for (α, α) scattering and in refs. [4–7] and their subsidiary references for (p, p) scattering.

The purpose of this paper is to present a data base of experimental (p, p) cross sections for isotopically natural C, O and Si at laboratory angles of 170°, 150° and 110°. Precise measurements of the elastic cross sections from natural targets at these angles are not available in the literature. The choice of the angle depends on the type of analysis performed. Cross section increases at larger angles therefore, in our laboratory, 170° is used for optimum elemental mapping, 110° for optimum depth profiling and 150° for routine work.

The present data base can be used to fit experimental proton BS spectra from samples of unknown composition as well as routine simulations.

2. Theoretical discussion

The formation of a resonance at a particular incident energy may be associated with the formation of an excited multinucleon compound system composed of the projectile and the target nucleons. This occurs when the incoming nucleon has sufficient energy in the centre of mass frame approaching the Coulomb barrier height of the target nucleus, so that it penetrates the barrier and interacts strongly with the target nucleus wherein the short range nature of the strong interaction localises the compound nucleus to a small region of the configuration space of the multiparticle system [8]. The resonances observed in the cross section data are due to the eigenstates of the compound nucleus. The structure of the resultant resonant states is defined by Breit and Wigner [9] who derived the well known formula for the energy dependence of the cross section close to resonance.

R-matrix theory, developed by Wigner and Eisenbud [10], incorporates the compound nucleus mechanism as well as other reaction channels. It solves the many body scattering problem by expanding the internal region solution in a basis set and matching this to the known, simple two body external solution. This leads to specific tests of microscopic models of nuclear structure [11]. In the case of elastic proton scattering by light nuclei, the cross section is the result of Coulomb (Rutherford) scattering at low energies, nuclear scattering at energies above the Coulomb barrier (non-Rutherford) and interference between the Coulomb and nuclear potentials which produces smooth variation in the background.

At energies below 2 MeV, the s-wave ($l = 0$) makes the main contribution to the background cross sections. However, at higher energies, p-waves ($l = 1$) begin to influence the empirical cross sections. Sometimes, two nearby resonances can interfere and this could affect the background. Some theoretical calculations employ a potential scattering background instead of the usual hard sphere scattering background. Background corrections indicate that either square well or Woods–Saxon wave functions are preferable for the description of the single particle states [8].

For analytical purposes, use of an experimental measurement of the shape of the resulting cross section is more satisfactory than analytical computation, since the shape is not readily computed by simple analytical methods. This is particularly the case for a natural target composed of a mixture of isotopes. Therefore, tables of Breit–Wigner parameters are presented here which can be used to calculate measured cross sections at any energy between 1.0 and 3.6 MeV.

3. Experimental

Proton and α beams were delivered by the University of Melbourne 5U Pelletron accelerator. Energy selection was provided by a 90° analysing magnet, the field strength of which was monitored by means of a nuclear magnetic resonance probe. A quadrupole doublet, located approximately halfway between the analysing magnet exit slits and the target chamber, together with a collimator at the entrance to the target chamber, was used to focus a beam spot a few mm in diameter on the target.

Two kinds of particle detectors were used: an Ortec surface barrier detector with an energy resolution of ~ 14 keV, area of 100 mm^2 and solid angle, Ω, of ~ 3 msr was used at 150° and Canberra Packard PIPS (passivated implanted planar silicon) detectors with FWHM ≤ 11 keV, areas of 100 and 50 mm^2, $\Omega \sim 3$ and 1.6 msr were positioned at 170° and 110°, respectively. The angular position of the detectors was known to $\pm 0.5°$. No aperture was needed in front of the detectors, since the solid angle was small and variations in the kinematic factor over the face of the detectors were < 5 keV which were negligible.

For the Si and O cross section measurements two nearly identical targets having natural isotope abundances were used. They consisted of a thick glassy carbon substrate with ~ 600 Å gold sputtered on the top and a ~ 1500 Å layer of Si_1O_x ($x \sim 1$) was sputtered over the gold layer.

For C cross section measurements, two thin self-supporting carbon films ~ 2000 Å which were sputtered with ~ 160 Å of Au were used. The carbon film was positioned such that the gold layer was facing the incoming beam. This was done so that the carbon buildup on the target could be monitored. The signal due to carbon buildup could be resolved from the main carbon peak because of the intervening Au. However, no significant carbon buildup was observed on the front surface of either target during the measurements. It was assumed from this that no significant carbon buildup occurred on the back surface either and hence the present measurements can be assumed to be free from systematic errors due to changes in the carbon thickness during the measurement.

A typical backscattering spectrum of 2.15 MeV protons incident on the $C/Au/SiO_x$ target and detected at 170° is shown in fig. 1. This shows backscattered signals from O, Si and Au which were integrated to determine the cross section as described below. The signals are completely resolved from the carbon plateau from the stopping thickness of the carbon substrate.

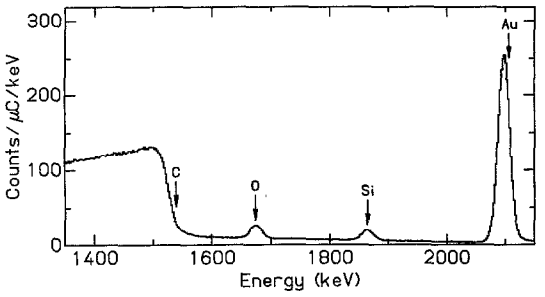

Fig. 1. A typical proton BS spectrum analysed to determine the cross section for (p, p) scattering from O and Si. In this case the proton bombarding energy was 2.15 MeV and the detector was at a scattering angle of 170°. The purpose of the Au signal is discussed in the text.

The thin layer of gold which was added to the targets allowed for simultaneous observation of Rutherford scattering from gold nuclei as a normalisation method, as described below. The thickness of the Au layer, along with the composition of the other layers of the targets, was determined by Rutherford backscattering spectrometry (RBS) with 2 MeV α-particles, using the surface energy approximation [12]. This analysis was done both at the beginning and end of each experiment to check whether there was any evidence of target depletion. No significant change in the target thickness and purity was observed.

For the cross section measurements, the target current was varied between 30–150 nA at proton beam energies of 1.0 to 3.6 MeV. The energy was stepped in minimum 2 keV and maximum 50 keV increments at

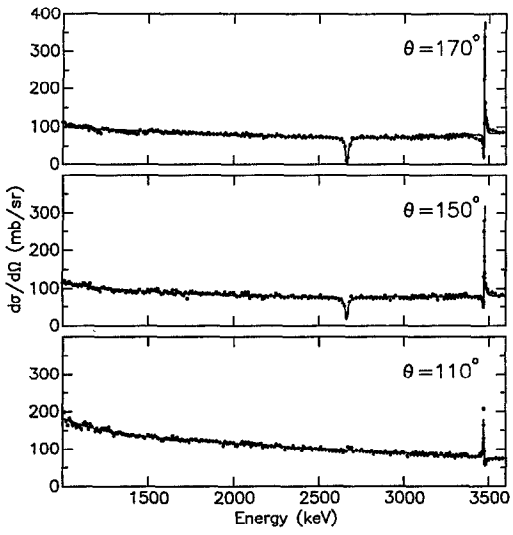

Fig. 3. The measured cross sections (dots) and empirical fits with Breit–Wigner functions for natural O in the laboratory frame.

narrow resonances and featureless portions of the excitation curves, respectively.

4. Analysis of the data and results

The signals from the elements of interest were integrated and then normalised by the yield from the Au layer. The surface energy approximation was valid since there was a negligible change in the beam energy

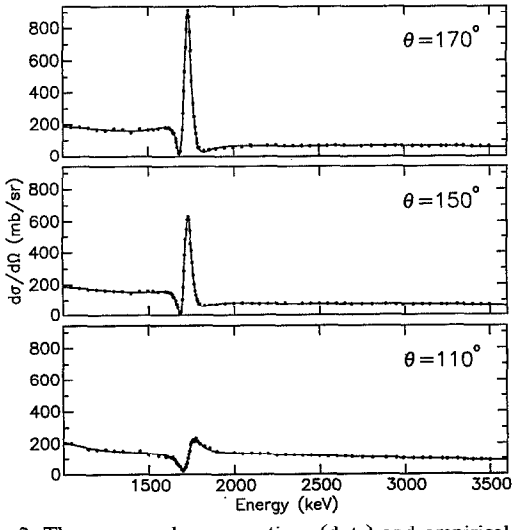

Fig. 2. The measured cross sections (dots) and empirical fits with Breit–Wigner functions for natural C in the laboratory frame.

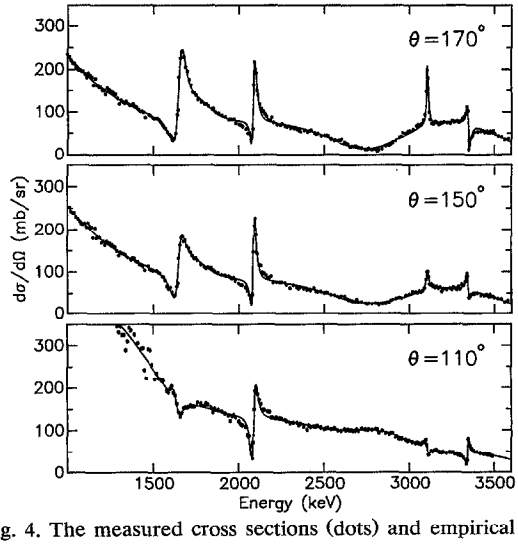

Fig. 4. The measured cross sections (dots) and empirical fits with Breit–Wigner functions for natural Si in the laboratory frame.

Table 1
Parameters of fit for carbon C(p, p)C

Breit–Wigner functions		
Height [mb]	Position [keV]	Width [keV]
110°, linear part 272.6 [mb], − 0.1220 [mb / keV]		
1530.8	−651.61	897.69
−123.83	1190.8	−1323.8
−913.48	1722.8	116.68
886.28	1723.9	119.79
292.62	4474.5	3929.9
150°, linear part 303.40 [mb], -5.692×10^{-2} [mb / keV]		
287.70	1694.4	231.74
−281.73	1689.5	56.682
938.81	1730.3	67.615
−588.17	1731.9	166.85
−103.57	1973.6	2264.6
170°, linear part 292.03 [mb], -5.841×10^{-2} [mb / keV]		
142.48	1647.2	266.55
−288.87	1686.4	47.284
1078.0	1731.2	54.826
−317.63	1750.0	183.01
−100.18	2039.5	1921.1

as it traversed the surface Au film. The absolute cross section for each element was calculated using [12]:

$$\left(\frac{d\sigma}{d\Omega}\right)_i = \frac{A_i}{A_{Au}}\left(\frac{(Nt)_{Au}}{(Nt)_i}\right)_\alpha \left(\frac{d\sigma}{d\Omega}\right)_{Au},$$

where A_i and A_{Au} are the number of counts in the BS spectrum for element i and Au at each energy. $(d\sigma/d\Omega)_{Au}$, is the Rutherford cross section for protons scattered off Au. This equation above can be rewritten as:

$$\left(\frac{d\sigma}{d\Omega}\right)_i = \frac{A_i}{A_{Au}}\left(\frac{A^\alpha_{Au}}{A^\alpha_i}\frac{\sigma^\alpha_i}{\sigma^\alpha_{Au}}\right)\left(\frac{d\sigma}{d\Omega}\right)_{Au},$$

where A^α_i is the peak area from 2 MeV α RBS and σ^α_i is the Rutherford cross section calculated at 2 MeV for a particular detector geometry for element i. Since the yields were normalised to Au, charge integration and solid angle did not enter in the above equations and therefore, systematic errors due to charge integration and dead time losses were also cancelled. The data was taken in two separate runs to monitor reproducibility of the data. The statistical error in the number of counts was better than 2% near resonances and better than 1% elsewhere. The reproducibility of the data was found to be 3% for most of the repeated data points. Corrections were made for the energy loss of protons and α-particles traversing the gold film in the carbon target and in C/Au/SiO_x due to energy loss in the SiO_x layer.

The occurrence possibility of inelastic proton scattering and other proton induced reactions which were negligible in the present measurements has been discussed in refs. [4,5]. This is because the cross sections measured are dominated by elastic proton scattering at low energies and other reactions or inelastic scattering are either energetically impossible or the reaction cross sections are a few orders of magnitude smaller than (p, p) cross sections.

The cross sections are mainly due to the most abundant isotope in the natural targets since the interaction probability of protons is the greatest with the most abundant isotope. This is not to say that rare isotopes are not contributing to the overall cross sections but these effects mainly raise the background.

Figs. 2–4 present the cross section data for C, O and Si, respectively. These data have been fitted with the Breit–Wigner resonance formula

$$\left(\frac{d\sigma}{d\Omega}\right) = a_0 + a_1E + \sum_j \frac{H_j(\Gamma_j/2)^2}{\left((E-E_j)^2 + (\Gamma_j/2)^2\right)},$$

where a_0, a_1 are the parameters of the linear contribution, H_j (height), Γ_j (width) and E_j (position) are the parameters of the resonance contribution with j taken to include as many terms as necessary to achieve a fit to the experimental cross sections to generally within 2%. We attach no special physical significance to the parameters of this function, they were determined simply to fit the data so that the cross section curves may be conveniently included in computations aimed at the simulation of BS spectra. The parameters of the fits to the cross section data for the three detector angles are given in tables 1, 2 and 3, respectively.

Table 2
Parameters of fit for oxygen O(p, p)O

Breit–Wigner functions		
Height [mb]	Position [keV]	Width [keV]
110°, linear part 156.99 [mb], -2.345×10^{-2} [mb / keV]		
241.26	579.57	427.71
242.83	3470.6	0.6978
−68.356	3473.1	12.898
85.933	3469.6	10.740
150°, linear part 29.112 [mb], 1.0756×10^{-2} [mb / keV]		
257.040	−437.44	1834.5
−60.957	2662.3	22.450
−361.722	3472.5	1.7722
348.07	3472.1	15.013
170°, linear part 99.94 [mb], -2.932×10^{-2} [mb / keV]		
238.19	−39273	20286
−77.27	2663.9	17.84
170.33	4887.9	2380
−317.7	3471.5	10.2
357.6	3472.5	2.24
261.4	3473.7	11.67

From the experimental data it is evident that the cross section varies with the scattering angle. This is to be expected since in the theoretical calculation of the cross sections, the complex scattering amplitude, $f(\theta)$ is dependent on Legendre polynomial series of each l value and this is the origin of angular dependence. This is of most significance for the 1.734 MeV resonance in carbon, $J^{\pi} = (\frac{5}{2})^{+}$, $l = 2$, which has a strong angular dependence. Therefore, in the analysis of carbon in a particular sample near this bombarding energy, more accuracy is achieved if the angular position of the detector is known to the highest accuracy. For resonances in oxygen and silicon this sensitivity is less marked.

5. Applications

As it was mentioned earlier, proton BS data has many potential applications. A silicon-on-insulator (SOI) structure has been analysed for depth profiling and mapping of SiO_2 regions using a 3 MeV proton microbeam [13]. The beam energy was tuned such that the oxygen signal was enhanced over silicon since the oxygen cross section at 3 MeV and below is larger than silicon, hence a better signal-to-noise ratio in the images was obtained, see fig. 3 in ref. [13]. The BS spectrum from the SOI structure was previously simulated using the literature data, however, now it could be simulated to greater accuracy, using the present data base.

Silicon carbide (SiC) has potential use in electronic and optical devices because of its high temperature stability, wide bandgap and high electron mobility [14]. Recently [15], SiC crystals have been analysed by a 3 MeV proton microbeam at 150°, see fig. 5, as shown here. The experimental spectrum is compared to a simulation calculated from the present data base. It is in excellent agreement with the experimental spectrum except for the carbon edge and this is possibly an indication of carbon buildup on the surface during the experiment or departure from stoichiometry of the sample.

One of the most interesting applications of proton BS is to measure oxygen concentration in high T_c superconductors (HTS), since the superconducting state is very sensitive to the oxygen content. Refs. [16,17] present results of the analysis of Y–Ba–Cu–O (YBCO) superconductors with α and proton beams. Ref. [18] studies different ion beams (protons, alphas as well as heavy ions) in different energy ranges for both thin and thick samples.

However, measurement of the oxygen content can be difficult because the oxygen signal appears superimposed on the large signal from the heavy components of the samples. Despite this, it is possible to get accurate results by exploiting the large O(p, p)O cross sections around 3 MeV. Fig. 6 shows a proton BS at 2 MeV incident on a stoichiometric single crystal of $Y_1Ba_2Cu_3O_{7-\delta}$. The actual spectrum was taken at 155° but the simulation is done using the new O(p, p)O data base for 150°. This will not affect the simulation since the cross section at 155° differs only slightly from 150° as mentioned earlier in the discussion of angular distributions. The simulation is for $Y_1Ba_2Cu_3O_7$ and as it can be seen, oxygen simulation is in excellent agreement. The inset in fig. 6 shows the same simulation done with the assumed oxygen stoichiometries of

Table 3
Parameters of fit for silicon Si(p, p)Si

Breit–Wigner functions		
Height [mb]	Position [keV]	Width [keV]
110°, linear part	*– 732.6 [mb], 0.02540 [mb / keV]*	
3927.6	397.87	836.50
–1326.3	1629.3	73.048
1310.2	1628.4	70.310
–132.33	1210.2	–172.50
–1738.4	2086.9	41.754
1717.8	2088.5	42.013
711.88	2917.2	3926.4
62.104	3106.3	38.913
–65.382	3112.7	29.032
–79.583	3146.3	667.35
–42.247	2564.5	549.00
764.44	3346.8	24.350
–754.17	3346.1	–24.704
150°, linear part	*– 694.31 [mb], 8.766 × 10 $^{-2}$ [mb / keV]*	
1270.9	66.731	2029.5
–1299.3	1651.7	88.423
1317.2	1655.1	85.757
43.046	1742.9	215.85
132.47	2039.6	2850.1
–1626.1	2084.3	34.001
1688.0	2085.9	33.698
–359.21	2801.2	1192.4
46.511	3108.1	18.889
748.79	3345.7	23.137
–737.78	3346.4	–23.127
170°, linear part	*– 696.69 [mb], 8.7123 [mb / keV]*	
1246.4	41.493	2035.6
–1269.3	1650.7	92.656
1349.5	1655.6	88.022
55.955	1759.8	227.03
128.09	2063.7	3173.9
–1627.2	2083.0	35.530
1687.4	2084.6	35.648
577.08	2867.4	1849.9
–361.78	2780.8	1043.1
139.01	3105.9	12.742
741.07	3344.0	24.543
–747.16	3346.3	–24.662

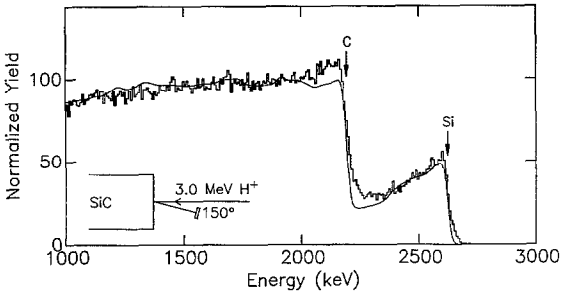

Fig. 5. An experimental proton BS spectrum from a SiC crystal (histogram) together with a simulation (smooth curve) utilising the present measured Si and C cross sections. The simulation in this and subsequent figures was performed with a modified version of RUMP [22].

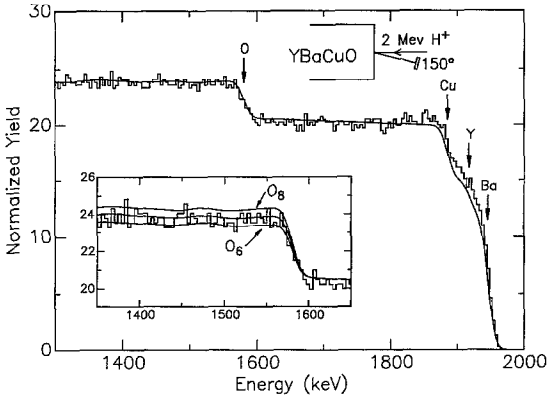

Fig. 6. An experimental proton BS spectrum from a YBCO crystal (histogram) together with a simulation (smooth curve) utilising the present measured O cross sections assuming sample composition $Y_1Ba_2Cu_3O_7$. The inset compares simulations for different O compositions.

O_8 and O_6. Relatively small departures from the actual stoichiometry, close to O_7, could be seen very clearly.

Fig. 7a shows a spectrum of a nonstoichiometric and possibly multiphased sample of YBCO taken at 170° with an incident proton beam energy of 3.60 MeV. The simulation from the present data base was fitted to the experimental spectrum and the stoichiometry was determined to be: $Y_1Ba_{1.5}Cu_{2.4}O_{5.5}$ with sulfur contamination. The oxygen resonance at 3.473 MeV is seen as a small peak on the experimental spectrum. The resonance is smeared out due to the straggling effects and this is not taken into consideration in the simulation program.

Fig. 7b is the same sample taken using a 2 MeV α beam. The oxygen surface edge is barely visible and this is due to low O(α, α)O cross section in the vicinity of 2 MeV. The relative Y, Ba and Cu concentrations were determined from their heights of the leading edges in this spectrum and used for the simulation shown in fig. 7a. Thus the concentration of all the elements, including oxygen, were determined from the spectra shown in figs. 7a and 7b. The present data base has potential applications in the study of ion beam induced damage in HTS for monitoring changes in oxygen stoichiometry or crystallinity since previous studies have shown that irradiation leads to an enhancement in the critical current density (J_c) and normal state resistivity (ρ) [19,20].

The present cross sections may also be potentially used to measure the carbon and oxygen content of biological specimens, allowing accurate measurement of trace element concentrations in cells, where the trace element signals have been detected simultaneously by PIXE. For example, fig. 6 in ref. [21] shows a backscattering spectrum obtained on a plant with an incident proton energy of 3 MeV and the signals due to C and O are well separated and suitable for analysis with the present cross sections.

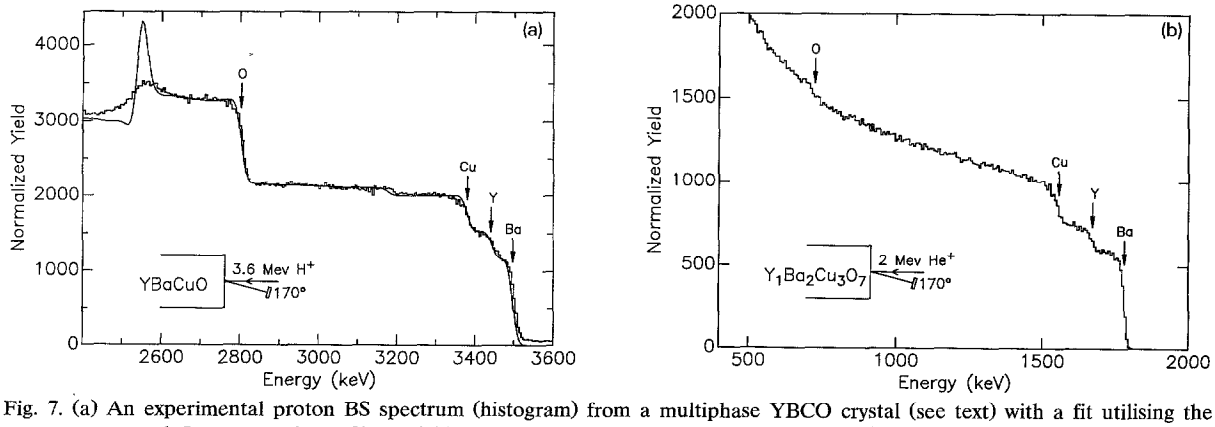

Fig. 7. (a) An experimental proton BS spectrum (histogram) from a multiphase YBCO crystal (see text) with a fit utilising the present measured O cross sections. The stoichiometry of the metals was determined from (b). (b) Conventional α-particle RBS spectrum from the sample of (a) showing the very poor signal-to-noise ratio of the O signal.

The examples given in this section demonstrate the reliability and accuracy of the new data base for future research in microanalysis of materials.

Note

The measured cross sections and the fit parameters are available by anonymous ftp from tauon.ph.unimelb.edu.au (IP address 128.250.50.2), subdirectory pcross, or alternatively by mailing a blank high density disk to the second author.

Acknowledgements

The authors wish to acknowledge the help of Dr. P. Kemeny of the Telecom Australia Research Laboratories for providing the SiO_x film, Mr. D. Dryden for assisting with the Au deposition and Mr. R. Szymanski for help with the accelerator operation. R. Amirikas would also like to thank S.G. Tims and R.A. Brown.

References

[1] S.P. Dooley, D.N. Jamieson and S. Prawer, these proceedings (3rd Int. Conf. on Nuclear Microprobes, Uppsala, Sweden, 1992) Nucl. Instr. and Meth. B77 (1993) 484.
[2] J.A. Leavitt and L.C. McIntyre, Jr., Nucl. Instr. and Meth. B56/57 (1991) 734.
[3] L.C. McIntyre, Jr., J.A. Leavitt, M.D. Ashbaugh, Z. Lin and J.O. Stoner, Jr., Nucl. Instr. and Meth. B64 (1992) 457.
[4] E. Rauhala, Nucl. Instr. and Meth. B12 (1985) 447.
[5] E.Rauhala, Nucl. Instr. and Meth. B40/41 (1989) 790, and refs. therein.
[6] J.M. Knox, Nucl. Instr. and Meth. B66 (1992) 31 and refs. therein.
[7] R. Amirikas, 4th Year Report, Univ. of Melbourne (1991) unpublished.
[8] L. Rikus, Ph.D. Thesis, Univ. of Melbourne (1980) unpublished.
[9] G. Breit and E.P. Wigner, Phys. Rev. 49 (1936) 519.
[10] E.P. Wigner and L. Eisenbud, Phys. Rev. 72 (1947) 29.
[11] A.M. Lane and R.G. Thomas, Rev. Mod. Phys. 30 (1958) 257.
[12] W.K. Chu, J.W. Mayer and M.A. Nicolet, in: Backscattering Spectrometry (Academic Press, New York, 1978).
[13] D.N. Jamieson, G.W. Grime and F. Watt, Nucl. Instr. and Meth. B40/41 (1989) 669.
[14] H. Sekiguchi, T. Nishijima, I. Nashiyama, N. Kobayashi, T. Misawa and S. Yoshida, Nucl. Instr. and Meth. B54 (1991) 225.
[15] M. Cholewa, A. Saint, G.J.F. Legge, D.N. Jamieson and T. Nishijima, these Proceedings (3rd Int. Conf. on Nuclear Microprobes, Uppsala, Sweden, 1992) Nucl. Instr. and Meth. B77 (1993) 184.
[16] J.A. Leavitt and L.C. McIntyre, Jr., Nucl. Instr. and Meth. B40/41 (1989) 797.
[17] K.K. Bourdelle, Nucl. Instr. and Meth. B66 (1992) 274.
[18] E. Rauhala, J. Saarilahti and N. Nath, Nucl. Instr. and Meth. B61 (1991) 83.
[19] W.-K. Chu, J.R. Lui and Z.H. Zhang, Nucl. Instr. and Meth. B59/60 (1991) 1447.
[20] J.C. Barbour, E.L. Venturini, D.S. Ginley and J.F. Kwak, Nucl. Instr. and Meth. B65 (1992) 531.
[21] Ph. Massiot, F. Sommer, M. Thellier and C. Ripoll, Nucl. Instr. and Meth. B66 (1992) 250.
[22] L.R. Doolittle, Nucl. Instr. and Meth. B9 (1985) 344.